GEOLOGIAN TUTKIMUSKESKUS
MTM
Espoo

6.6.2019 17/2019

High Purity Quartz (HPQ); Mineralogical, Geochemical and Potential Occurrences in Finland

Thair Al-Ani, Sari Grönholm, Esa Pohjolainen and Jukka Kuva

GTK

GEOLOGIAN TUTKIMUSKESKUS • GEOLOGISKA FORSKNINGSCENTRALEN • GEOLOGICAL SURVEY OF FINLAND

PL/PB/P.O. Box 96 FI-02151 Espoo, Finland
PL/PB/P.O. Box 1237 FI-70211 Kuopio, Finland
PL/PB/P.O. Box 97 FI-67101 Kokkola, Finland
PL/PB/P.O. Box 77 FI-96101 Rovaniemi, Finland

Puh. 029 503 0000 • Tel. +358 29 503 0000 • www.gtk.fi • Y-tunnus / FO-nummer / Business ID: 0244680-7

6.6.2019

GEOLOGICAL SURVEY OF FINLAND **DOCUMENTATION PAGE**

Date / Rec. no.

Authors Thair Al-Ani Sari Grönholm Esa Pohjolainen Jukka Kuva		Type of report arkistoraportti Commissioned by GTK	
Title of report High Purity Quartz (HPQ); mineralogical, geochemical and their potential occurrences in Finland			
Abstract Quartz samples of different origin from 18 localities in the Central and Southern Finland have been investigated to characterize their trace element compositions, mineral impurities and defect structures. The analytical combination of optical and scanning electron microscopy (SEM) along with feature analysis and spectrum imaging, X-ray computed microtomography (XCT) scanning & analysis, and trace-element analysis by XRF and ICP-MS. The results show that impurities within the quartz mainly include muscovite, albite, K-feldspar, Al/Fe oxides (clay), and secondary fluid inclusions. The main chemical impurities are Al (106-8890 ppm), K (25-3140 ppm), Fe (70-2660 ppm), Na (222-1110 ppm), Ca (21-930 ppm), and Ti (20-110 ppm). All the samples from deposits under this study do not meet the requirements of the HPQ definition and they are thus low purity quartz deposits. However a beneficiation study on these deposits is recommended to establish possible industrial applications that may be feasible. X-ray computed microtomography (X-μCT) is applied here to investigate in a non-invasive way the three-dimensional (3D) spatial distribution of fluid inclusions and internal structure (impurities, porosity, fractures, etc.,) of the quartz samples. XCT allows us to identify > 4 μm fluid inclusions while the identification and volumetric reconstruction of the different phases can be carried out with reasonable confidence for relatively large (> 25 μm) inclusions. The volumetric reconstruction of the liquid and vapor phases or porosity values calculated from the XCT images of four quartz samples are 0.87 %, 0.34 %, 0.16 % and 0.13 % respectively, with a mean value less than 1 %.			
Keywords: High Purity Quartz (HPQ), Mineralogy, Fluid inclusions, Internal structure, High-resolution X-ray CT and 3D analysis.			
Geographical area: Finland			
Map sheet			
Other information			
Report serial		Archive code 17/2019	
Total pages 24	Language English	Price	Confidentiality julkinen
Unit and section MTM		Project code 50402-2009022 WP2	
Signature/name Thair Al-Ani		Signature/name	

Contents

6.6.2019

1 INTRODUCTION

Quartz is one of the most abundant minerals and occurs in many different geological settings (Götze 2009). The demand for the raw material quartz is increasing worldwide, in particular, the demand for high-purity quartz (Haus 2010; Moore 2005; Dal Martello et al. 2011a, b). Therefore, high purity quartz has become one of today's key strategic raw materials for the high-tech industry. The trace-element contents of quartz are its most important quality criteria. Quartz is designated high purity when it contains not only less than 50μg g−1 of impurities, which mainly comprise structurally bound trace elements (B, Li, Al, Fe, Ti, Ca, K, Mg, Mn, Na and P) in the quartz lattice, but also micro inclusions of minerals and trapped fluids. The usual types of fluid inclusions are: a) Water containing, biphasic inclusions liquid-gas rich liquid phase, negative crystal shape. b) Coexistence rich inclusions in liquid and gas phase. c) Fluid inclusions that define growth zones in peculiar quartz. d) Decadent – broken inclusions in milk colored solid quartz, (Kilias et al. 2004) Ultra-pure is rare in nature and larger deposits even more so. HPQ is rare in nature and larger deposits even more so. The few HPQ deposits found around the world include certain types of quartz-rich granitic pegmatite (e.g. IOTA®2005; Norwegian Crystallites AS2006) and hydrothermal quartz veins.

Silica glass melted out of high purity quartz sand offers a wide range of exceptional optical, mechanical and thermal properties, which are essential for manufacturing many high-tech products in areas such as semiconductor technologies, high temperature lamp tubing, telecommunications and optics.

The present study presents results of a comprehensive mineralogical and geochemical study on potential HPQ deposits of different genetic types from 18 sites in the Central and Southern Finland (Fig. 1). The main objectives of this project will be:
- Exploration and evaluation of quartz occurs in pegmatite, hydrothermal vein and quartzite deposits in Finland, in order to assess their potential as future long term sources for different high – tech industries. Determination of mineralogical and chemical composition of selected quartz samples, in order to obtain detailed information about the type and abundance of lattice defects and contaminating trace elements of these quartz materials in order to determine the critical processes and conditions responsible for the formation of HPQ deposits.
- Use of multiple high-sensitivity analytical techniques ranging from optical to scanning electron microscopy, trace-element analysis by X-ray fluorescence spectrometry (XRF) with inductively coupled plasma mass spectrometry (ICP-MS) and advanced X-ray microtomography technology, which allow us to achieve stable and high resolution images of the internal structure (impurities, porosity, fractures, inclusions, grain size, etc.) of high purity quartz
- Study of the fluid inclusions in the quartz vein with main aim first of all to investigate the role of fluid inclusions as quality "contaminants" in terms of chemical composition, distribution density, morphology and size and secondly to determine the physiochemical conditions and mechanisms of vein crystallization and find out the pattern of fluid inclusions distribution.

6.6.2019

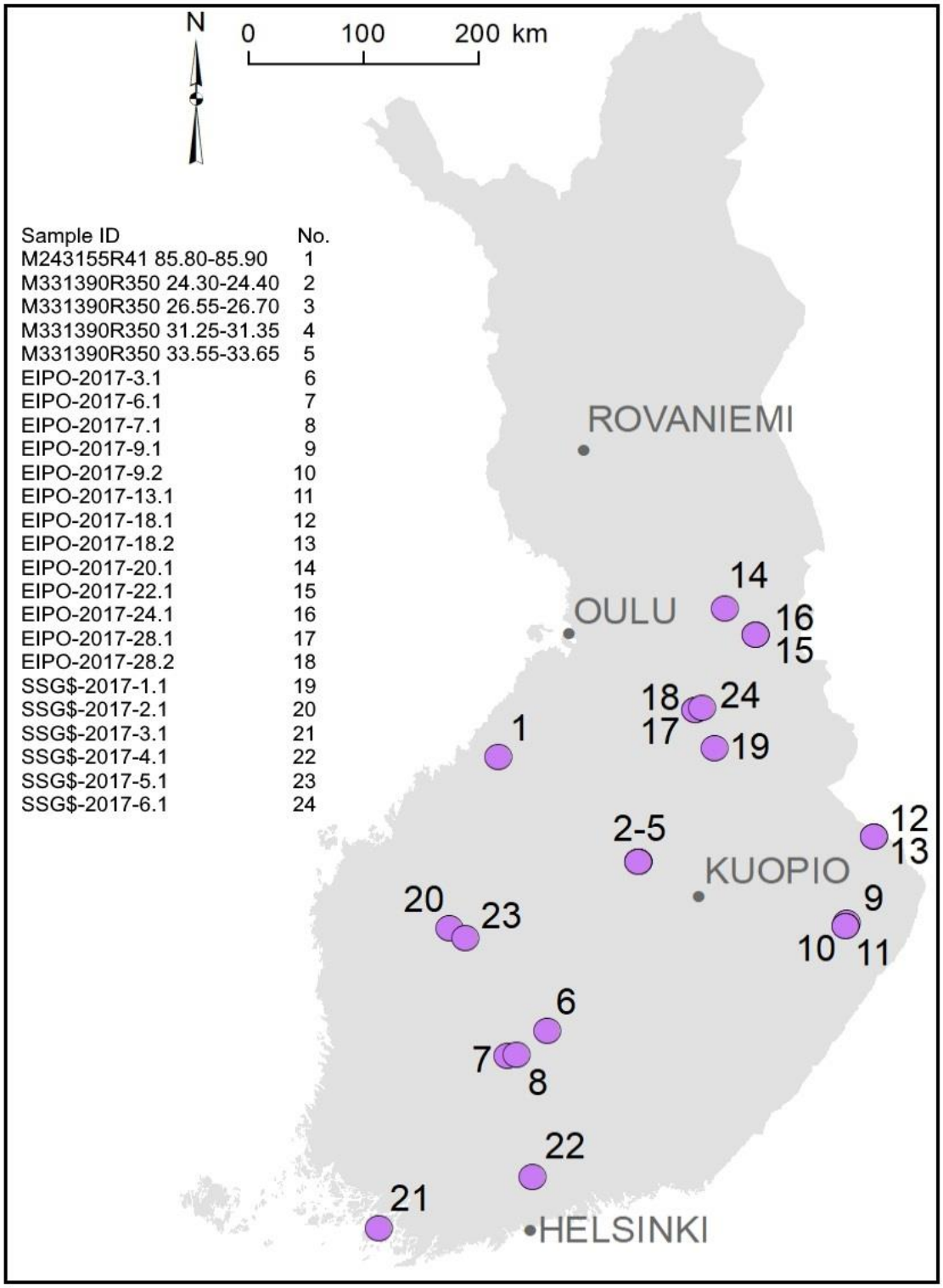

Figure 1. *Location of High Purity Quartz (HPQ) samples in Finland.*

2 HIGH PURITY QUARTZ RESOURCES

Nowadays, high purity quartz has become one of today's key strategic raw materials for the high – tech industry Sibelco-USA is the world's leading high purity quartz producer with deposits and operations in North Carolina, USA. One of the few alternative suppliers, Norwegian Crystallites, has been producing high purity quartz from its Drag plant in western Norway and several underground and open pit mines since mid-1996 when the company changed ownership. Following the acquisition of North Carolina K-T Feldspar (2001) and the Feldspar Corporation (2007) by French company IMERYS, Norwegian Crystallites and IMERYS joined to form the Quartz Corp. in 2011. Quartz raw material for high purity applications is mined just adjacent to one of the Unimin deposits in North Carolina, then shipped and refined into high purity quartz products at its Drag plant in Norway. Crystalline fillers and high purity quartz sand are produced and exported worldwide to the semiconductor, lighting and other industries. Although mined by two companies (Unimin Corp. and The Quartz Corp.), the geographical monopoly with only one major source for high purity quartz located in Spruce Pine, North Carolina, USA persists.

Potential new entrants into the high purity quartz world market are Moscow-based JSC Polar Quartz, with raw material supply based on the Neroika deposit on the eastern slope of the sub-polar (northern) Urals. After many years of stagnancy Rusnano, wholly owned by the Government of the Russian Federation, Ural Industrial Corporation, and Khanty-Mansiysk Autonomous Okrug signed a shareholders' agreement for the Polar Quartz project in 2011.

Kyshtym Mining (also known as KGOK or Russian Quartz), situated on the Eastern slopes of the South Ural Mountains, supplied 60% of domestic high purity quartz demand in the Soviet era. A project to technically refine and re-equip the manufacturing processes started in 2011 with financial support from Rusnano. In 2012 the first production line offering a capacity of 6,000 tons per year for dry concentration has been launched. One year later Rusnano announced its partial exit from Russian Quartz selling it to Sumitomo Corporation, a leading integrated business group headquartered in Japan (https://www.anzaplan.com/strategic-minerals-metals/high-purity-quartz/).

By the end of 2012, Nordic Mining released a Scoping Study, describing the current status of development in the Kvinnherad quartz project. During an advanced test program very low final impurity levels with improved melting behaviour were confirmed and reproduced for samples from different locations in the deposit.

Another recent project development located in Mauretania (North-Western Africa) has been presented by MMC (Mauretania Minerals Company) during the Silica Arabica 2012 event in Jeddah, KSA, with more than 150 quartz veins in the desert area and proven high.

3 RESEARCH MATERIALS AND METHODS

This research project was aimed at characterizing quartz from selected potential High Purity Quartz (HPQ) deposits in terms of impurities associations, associated trace element concentrations, and internal structure. Twenty four quartz rock samples were collected from different localities in Central and Sothern Finland, sometime with two samples collected from each locality (Fig. 1). Figure 2 given below shows quartz samples from the studied deposits. The study followed a route which enabled the researcher to achieve the following: firstly to determine whether the deposits under study meets HPQ requirements, and

secondly to acquire an understanding of growth features of the quartz grains which gives a reflection of the crystallization and recrystallization processes of the quartz. Methods and procedures used in the analysis of raw quartz samples are discussed in the following.

3.1 Optical microscopic studies

Optical microscopic studies of the sample (thin section) were carried by using model petrographic microscope (LEICA DMLP) equipped and image analysis was carried out using (Leica) application suite microscope Software. The images were obtained in both plane polarized light and cross polarized light at different magnifications such as 2.5X, 5X, 10X and 20X objectives. Petrographic examination identified various impurities, their sizes, occurrence and their distribution.

3.2 Scanning electron microscopy (SEM) studies

Investigation of samples by scanning electron microscopy (SEM) of HPQ samples allows detailed identification of individual minerals and impurities, such as grain size and distribution of grain size, grain morphology and association and the relative abundance of minerals in the investigated sample. The chemical composition of the mineral impurities was analyzed qualitatively by quantitatively by point analysis. Particle-by-particle scanning electron microscopy and point count of ~4000 grains per slide were integrated to provide the percentage of the quartz and associated minerals the studied samples. The scanning electron microscope results for all HPQ samples are listed in Appendix 1.

3.3 Bulk Chemical Composition

Major and trace-element concentrations of quartzite samples were determined by X-ray fluorescence spectrometry (XRF) and ICP-MS- instrumental methods analysis at Labtium Oy, Sodankylä (Labtium methods, see details www.labtium.fi).

3.4 X-ray tomography studies

- **Sample preparation and mounting:** Six quartz rock samples were collected from some potential high purity quartz (HPQ) deposits in Finland, and thus ideal for integrated high resolution X-ray CT scanner (HRXCT) studies. Micro piece of a quartz samples are required for high resolution 3D imaging and geometrical orientation of impurity minerals, fluid inclusions and porosity in the selected High purity quartz (HPQ) samples. Start by cutting a needle blade with a 3 × 1.5 × 15 mm diameter from quartz rock sample. A set of many needle blade with a 3 × 1.5 × 15 mm diameter were separated by cutting from all studied samples by using precision thin section cutting and grinding machine (Fig. 3a-d).
- **High resolution X-ray micro tomography:** HRXCT is increasingly being applied in mineralogy and ore petrology due to its ability to resolve the three-dimensional (3D) shape and spatial distribution of minerals and associated microstructural features different rock types, including e.g., 3D distribution of primary melt and fluid inclusions in garnet porphyroblasts (Parisatto et al., 2018), identification of mineral inclusions in diamonds (Nestola et al. 2012), 3D distribution of minerals and associated microstructural features in a metamorphic rock fabrics (Sayab et al., 2015, 2016,

2017). A more detailed and technical account of CT and its applications to geological materials can be found in Ketcham and Carlson (2001) or Cnudde and Boone (2013). In this study, we have used XCT scanner (GE phoenix v|tome|x s, from EP-TeQ), hosted in the Geological Survey of Finland (GTK), to spatially map the internal structure (impurities, porosity, fractures, etc.) of the quartz samples (Fig. 3c). X-rays from a tungsten target were used with the X-ray tube voltage set to 75-80 kV and the tube current set to 150-200 µA for the coarse scans and to 325 µA for the more detailed scans. No filter was used for the beam. We acquired 2700 views per 360°, with each view averaged over three exposures after a wait time of one exposure at each view for detector stabilization. This amounted to 3 s total exposure time per view for the coarse scans and 6 s total exposure time per view for the more detailed scans. Two larger samples and four needle blade samples measuring 3 × 1.5 × 15 mm were scanned separately (Fig. 3d). The 3-D images had a voxel size of 12-15 µm for the coarse scans and 1.17 – 1.48 µm for the more detailed scans. All datasets were corrected for ring artifacts. For the detailed scans the data was segmented using a marker-based watershed algorithm to determine the volume fractions of the impurities. Numbering of samples and the experimental setups adopted for the investigation of each of them are reported in Table 1.

Table 1. *Experimental X-ray microtomography (X-µCT) setup adopted for each of the investigated samples. MF = microfocus tube, NF = nanofocus tube, mod = focus mode for NF tube*

Sample	EIPO-2017-7.1	EIPO-2017-22.1	EIPO-2017-6.1	EIPO-2017-20.1	EIPO-2017-18.2	EIPO-2017-3.1
Thin section No.	180245	180248	180244	180247	180246	180249
X-ray tube	240 kV MF	240 kV MF	180 kV NF mod 2	180 kV NF mod 2	180 kV NF mod 2	180 kV NF mod 2
Acceleration voltage/ kV	80	75	80	80	80	80
Tube current / uA	150	200	325	325	325	325
Exposure Time / ms	1000	1000	2000	2000	2000	2000
Projections	2700	2700	2700	2700	2700	2700
Total time/ h	3	3	6	6	6	6
Resolution / um	12.15	15.26	1.17	1.33	1.48	1.48
Beam Hardening Correction	6	6.5	7	8	8	9

Figure 2. *Investigated quartz samples of the present study.*

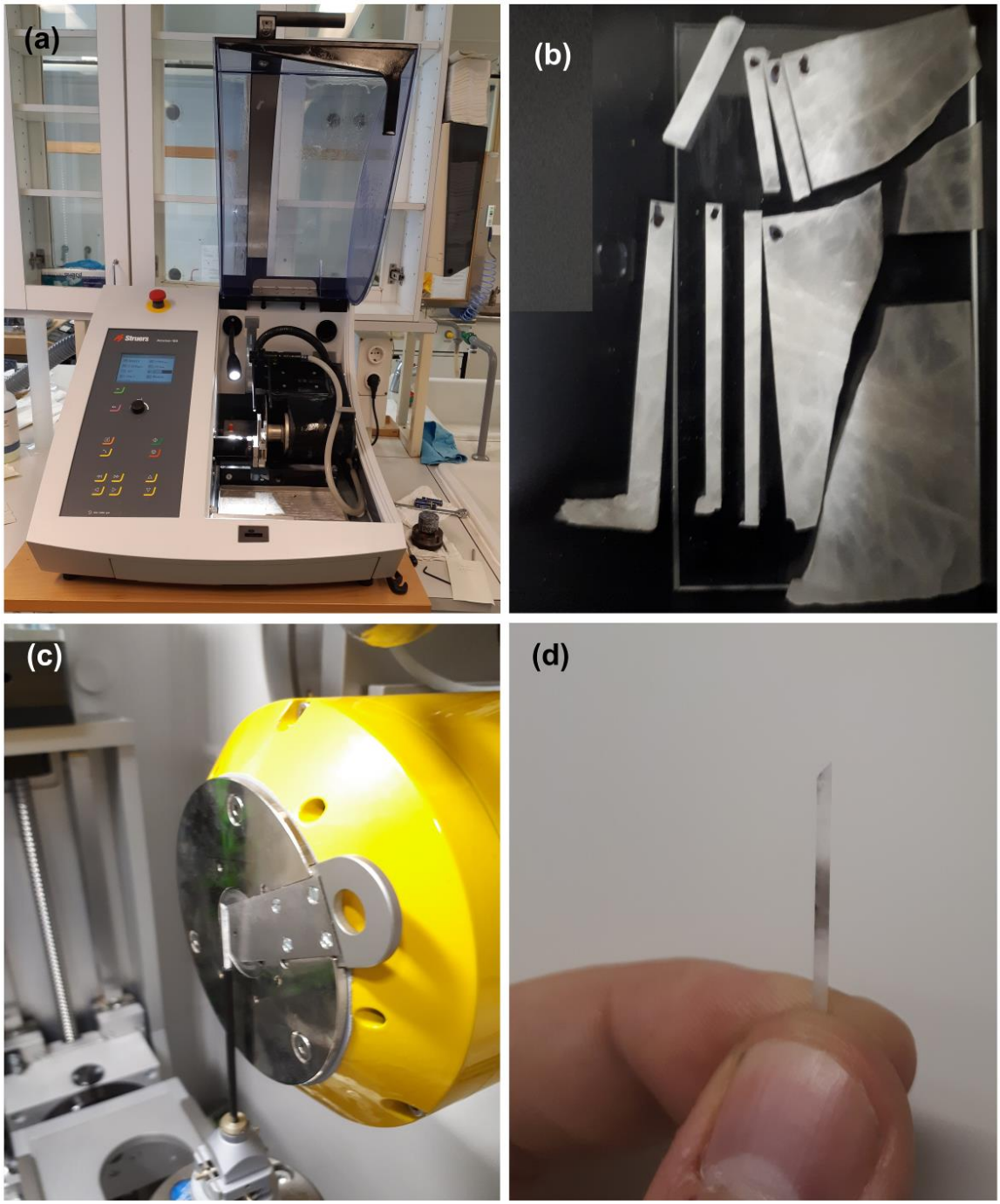

Figure 3. *Sample preparation steps for analysis by XCT scan; (a) Precision thin section machine for mineralogy; (b) Needle blade were separated by cutting from chip of quartz samples; (c) Quartz sample fixed close to X-ray source of a CT-scanning; (d) The part of the quartz sample that was exposed to X-rays appears as smoky black.*

4 RESULTS

Due to the ongoing exploration for high purity quartz in the many locations in Finland the analytical results are identified only by sample numbers without a reference to specific quartz deposits/veins.

4.1 Microstructures and petrography

Microstructural and petrography investigations of original samples using transmitted polarizing microscope revealed that the quartz samples are comprised mixture of multiple quartz generations. The primary igneous quartz occurs as coarse clear-to-smoky grains, which are partially or fully recrystallized into fine grained granular aggregates with a greatly increased surface area. This enhances fluid access during subsequent episodes of fracturing and fluid infiltration when multiple generations of hydrothermal quartz are formed by replacement along grain boundaries, as well as along fractures and veins (Fig. 4a, b). In thin-section, quartz grains consisted of subhedral to anhedral interlocked quartz crystals with particle size ranged from <50 μm to about 1000 μm and displaying elongate sub-grain boundaries. Quartz grains have inequigranular (uneven) to seriate (gradual and continuous variation in grain size) texture with anhedral edges and lobate grain boundaries (Figs. 4c, d). A variably developed spaced fracture cleavage is the only macroscopic evidence of the deformation within the quartzite (Fig. 4). Undulose extinction sweeps across most grains and extinction in deformation bands is common (Figs. 4 and 5). Note also here that the grain boundary textures from all of the quartzites samples indicate that recrystallization occurred by bulging recrystallization (e.g., Mancktelow and Pennacchioni, 2004). In transmitted light (Fig. 5a- d), grains depict seriate interlobate texture and intra- and inter- granular cracks of several generations as well as fluid inclusion trails are visible. The quartz was subjected to geological alteration; this is inferred by the presence of bulging recrystallization, subgrain rotation recrystallization, and grain boundary migration recrystallization.

The quartz samples showed to entrap impurities of solid, silicate melt and fluid inclusions. Solid inclusions were mainly muscovite, albite, K-feldspar, Al/Fe oxides (clay). Muscovite impurities were found either as minute inclusions in size range from <20 μm to 50 μm (Fig. 5a, b) or as muscovite long flakes inside the quartz crystals (Fig. 5a, b), or as micro fractures filling with size range from 10 to 120 μm (Fig. 6c, d). Sometimes they presented along the quartz grain boundaries in the form of micro-crystals with size range from 10 μm to 100 μm (Fig. 6e, f). Muscovite is commonly thought to be an important source of impurity elements, including Al, K, Mg, Fe and Ti.

Fluid inclusions are formed during the primary crystallization of quartz from cooling rock forming fluids and also as a result of secondary (re)-crystallisation processes related to tectonic events (Roedder, 1984). Fluid inclusion study is very important to know the condition of hydrothermal fluids and their origin. In general, fluid inclusions can be classified into monophase (liquid or vapor), two-phase (liquid+vapor or vapor+liquid), and multiphase (Roedder, 1984). Most of the fluid inclusions detected in random orientation inside the quartz crystals and commonly composed of two phases, (liquid+vapor) phase (Fig. 7a, b), and liquid-dominated phase with parallel orientation (Fig. 7c, d). The common size of fluid inclusions in this research is between < 5 to 20 μm. Fluid inclusions can also be classified into three types based on their genetic such as primary, secondary, and pseudo secondary. In this research, the most of fluid inclusions are trapped in the fractures which are developed after the formation of host mineral and caught due

of healing of fractures. These inclusions occur as trails or clusters which often cut across the grain boundaries and secondary in origin.

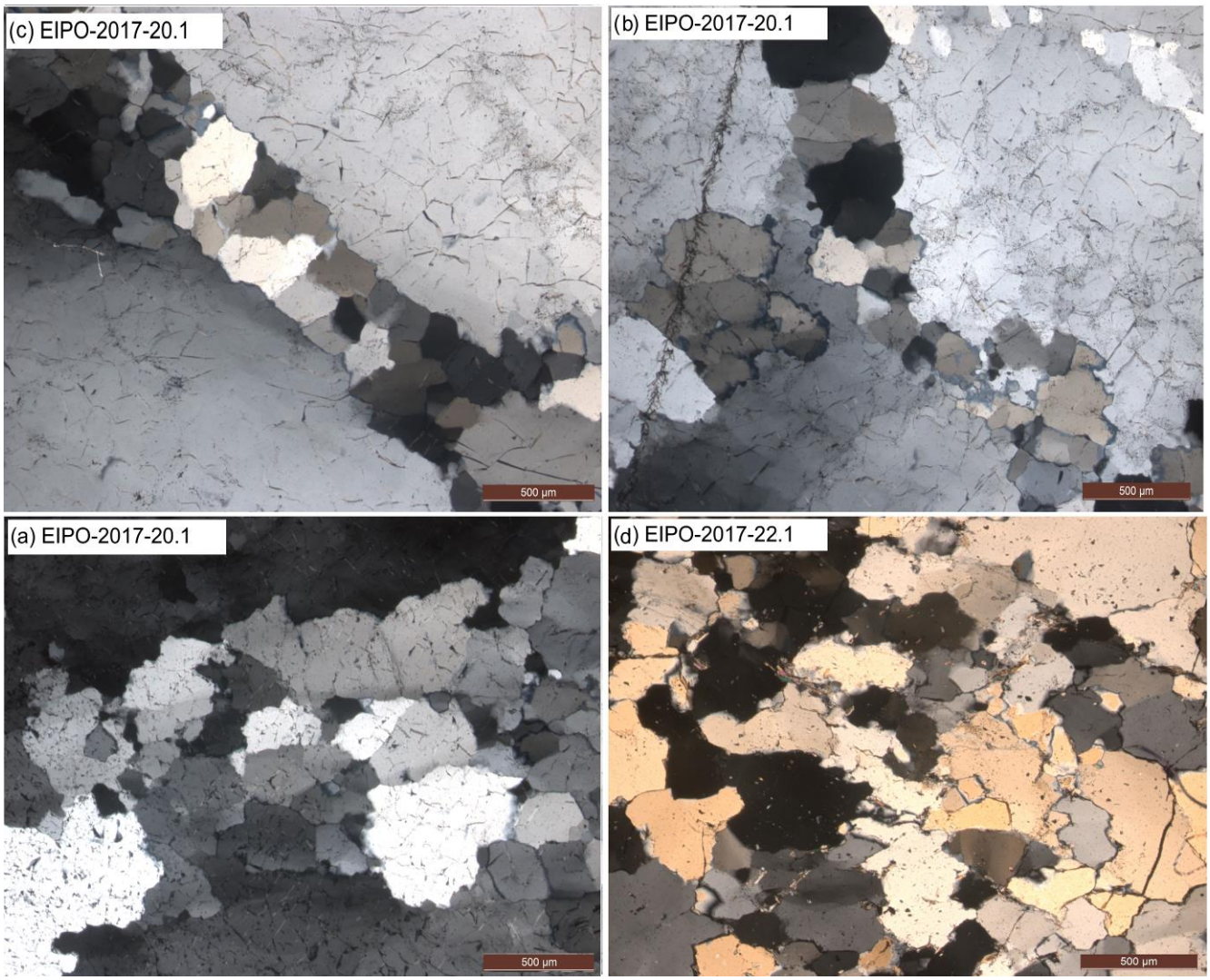

Figure 4. *Representative optical micrographs of quartz samples EIPO-2017-20.1 and 22.1; (a, b) The partial bulging recrystallization along fractures and veins; (c, d) Quartz grain boundaries as serrated, interlobated and sometime displaying irregularity of grain boundaries.*

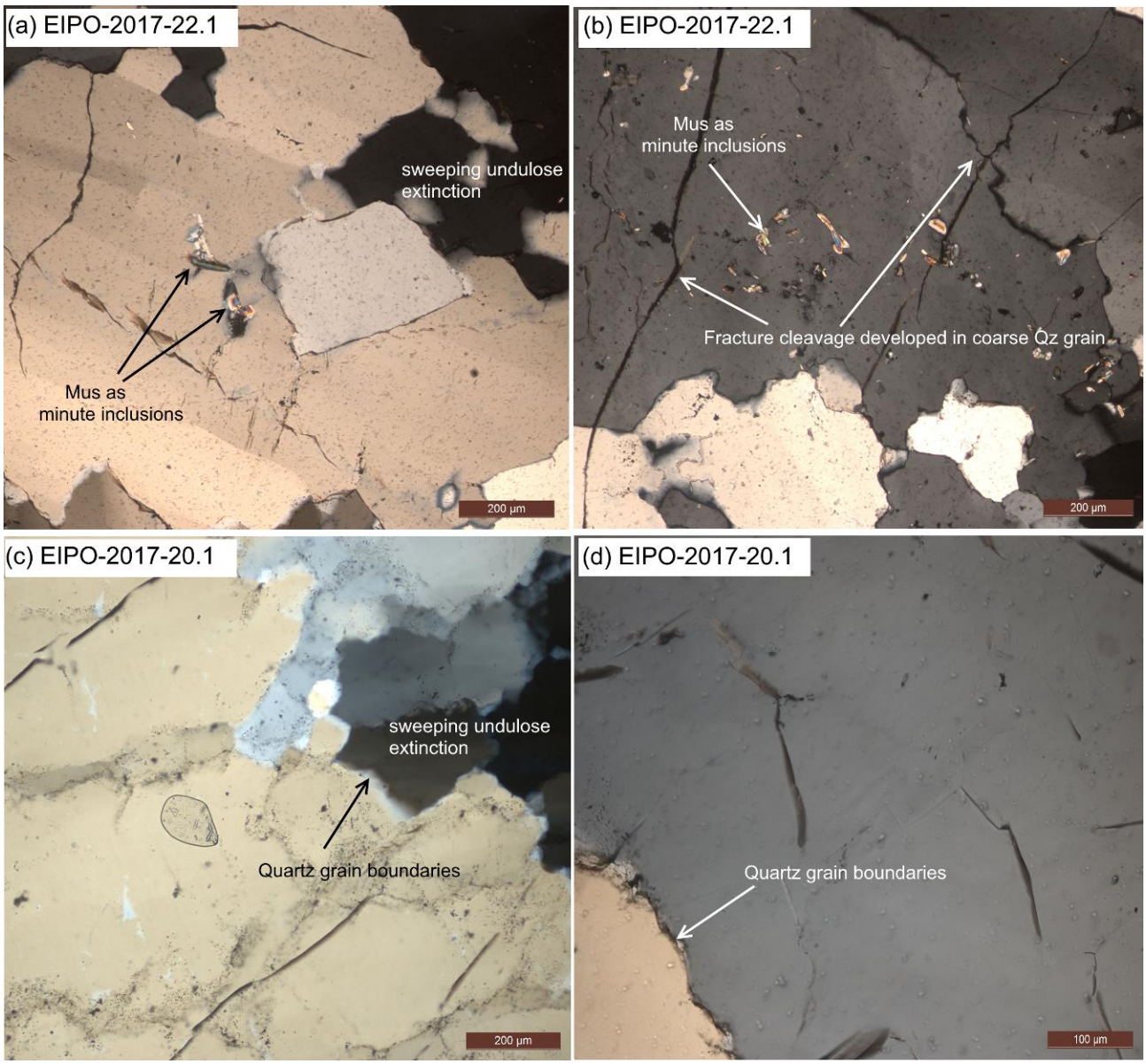

Figure 5. *Representative optical micrographs of quartz samples EIPO-2017-20.1 and 22.1, showing the developed spaced fracture cleavage within the quartz grains, sweeping undulose extinction and quartz grain boundaries.*

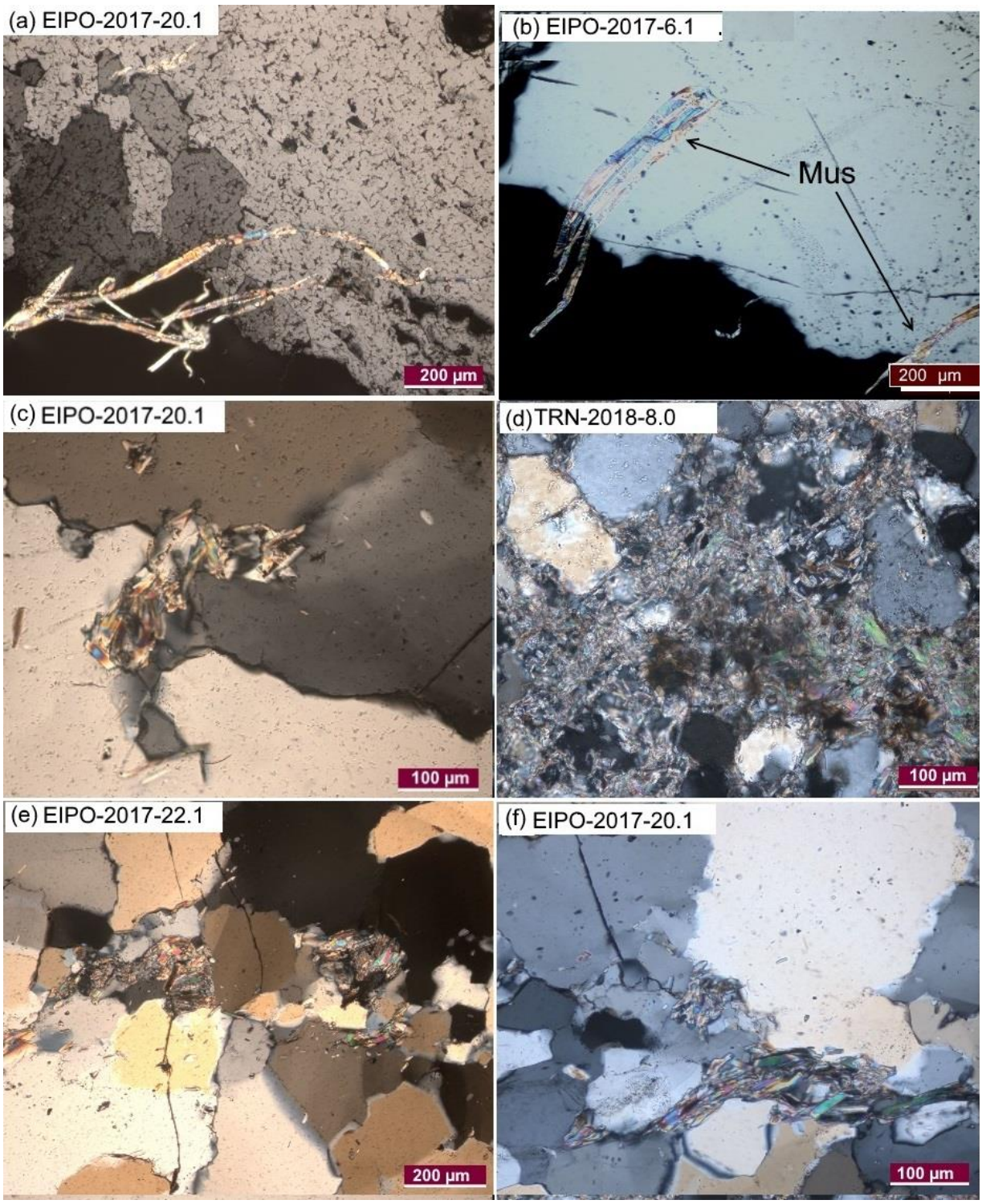

Figure 6. *Representative optical micrographs of some quartz samples showing; (a, b) Muscovite long flakes inside the quartz crystals; (c, d) Muscovite crystals present along grain boundaries; (e, f) Muscovite filling fractures within quartz.*

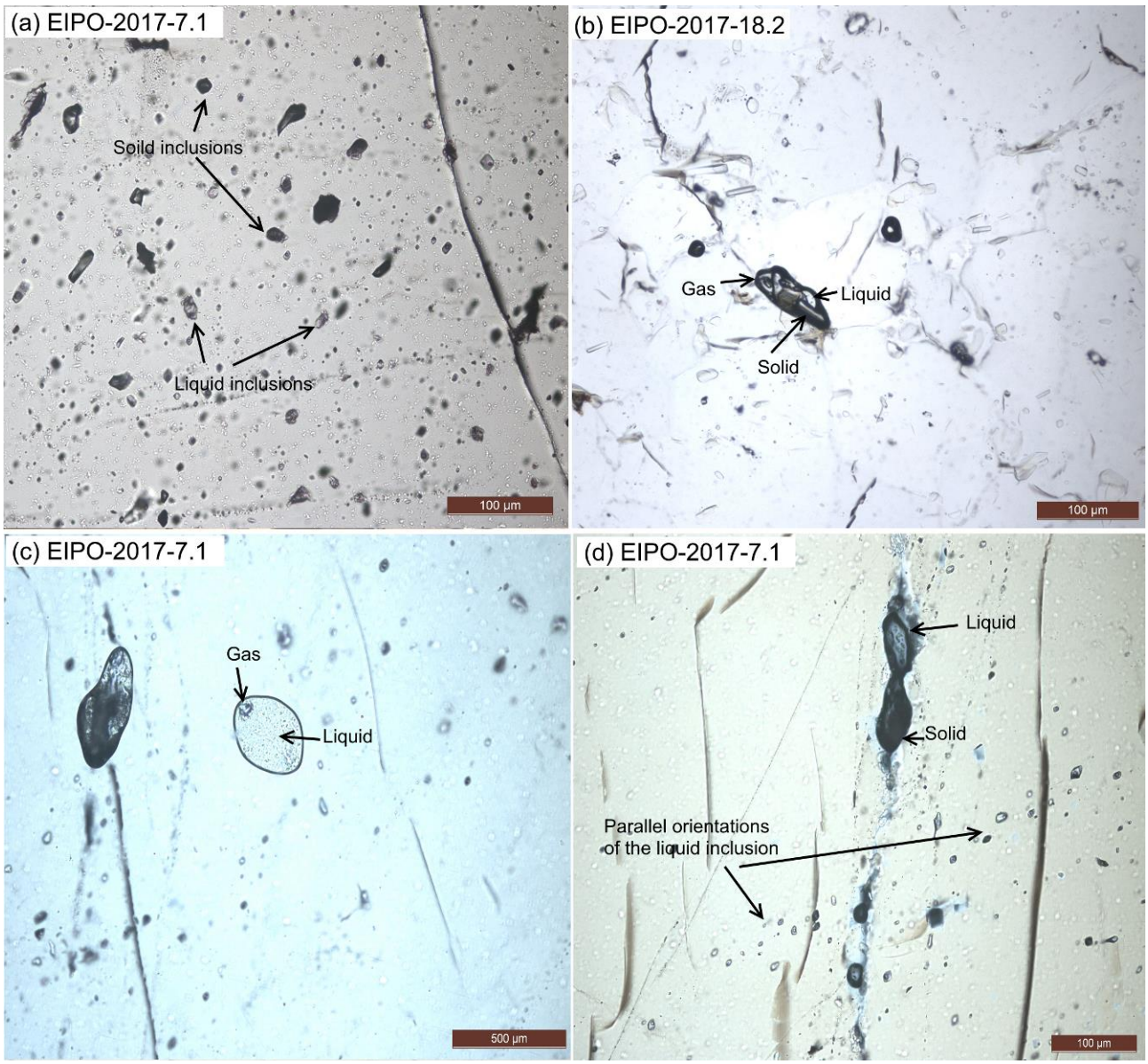

Figure 7. *Representative optical micrographs of quartz samples EIPO-2017-7.1 and 18.2; Fluid inclusions in some represented quartz samples; (a, b) secondary fluid inclusions detected in random orientation inside the quartz crystals and commonly composed of two phases, liquid phase and gaseous phase; (c, d) Parallel orientations of the fluid inclusion composed of two phases (liquid and gas).*

4.2 Chemistry and modal mineralogy by SEM

Although HPQ samples are petrographically determined with a polarizing microscope, further informations can be obtained by using scanning electron microscope (JEOL JSM 5900 LV). Typical properties of raw quartz that must be characterized are:

- Chemical composition of inclusions
- Size and morphology of inclusions
- Modal mineralogy

Based on a combination of optical microscope analysis and scanning electron microscope SEM analysis, the main mineral inclusions in the quartz are muscovite, albite, hematite and chlorite, as well as fluid inclusions (Fig. 8). The muscovite platelets are widely distributed along the quartz grain boundaries with size range from 20 μm to 200 μm (Fig. 8a, b), but a small quantity of muscovite is included in the quartz grains filling micro fractures within quartz crystals, in size range from <20 μm to 50 μm (Fig. 8c). The analysis (Table 2) shows that Al, K, Mg, and Fe are the major elements obtained in the muscovite and also in chlorite (Fig. 8b). Albite is also identified by SEM in some studied quartz samples shown in Fig. 8c. Its chemical analysis (Table 2) shows that the source of impurity elements, including Na, Mg and Al. Hematite and Fe/Al oxides are the main iron carrier in these veins, and mainly occurs filling thin cracks (Fig. 8d, f). Several observed grains have irregular boundaries and associated with cavities of variable shape and up to millimetre size along the open grain boundaries, which characterized by occurrences of muscovite crystals and sometimes filled by monazite, zircon and pyrite (Fig. 8e, f).

SEM imaging of quartz grain boundaries from studied sample shows that most of the grain boundaries are open on the nanometer scale. Three types of voids occur (i) roughly 50–500 nm wide open zones parallel to the grain boundaries. They are suggested to be caused by general volume reduction as a result of cooling stage of temperature (Fig. 9a, b); (ii) Cavities of variable shape and up to micrometer size along the open grain boundaries (Fig. 9b, c); and (iii) cone-shaped, micrometer-sized depressions at sites where dislocation lines meet the open grain boundaries (Fig. 9d). The latter two types are generated by dissolution–precipitation processes with iron oxides (Hem) filling some fractures (Fig. 9f). SEM images also show that fluid inclusions are either trapped in the fractures within the hosted grains or occurred as trails or clusters which often cut across the grain boundaries.

The quantitative modal abundance data provided by x-ray feature analysis in scanning electron microscopy SEM on the main mineral impurities indicated in selected quartz samples. X-ray feature analysis, particle-by-particle scanning electron microscopy and point count of more than 4000 grains per slide were integrated to provide the percentage of the mineral impurities in the studied samples. Table 3 presents the modal mineralogy of HPQ samples in selected the thin section and mineral grain counts. A total of 4000 grains were analyzed in the thin section of two samples EIPO-2017-7.1 and 20.1, showing high fluid inclusions content, but minerals impurities were not detected (Table 3). Modal mineralogy of other selected samples showed that the major impurity mineral species is muscovite with minor minerals such as albite Al/Fe oxides (clay), K-feldspar, hematite, zircon and monazite.

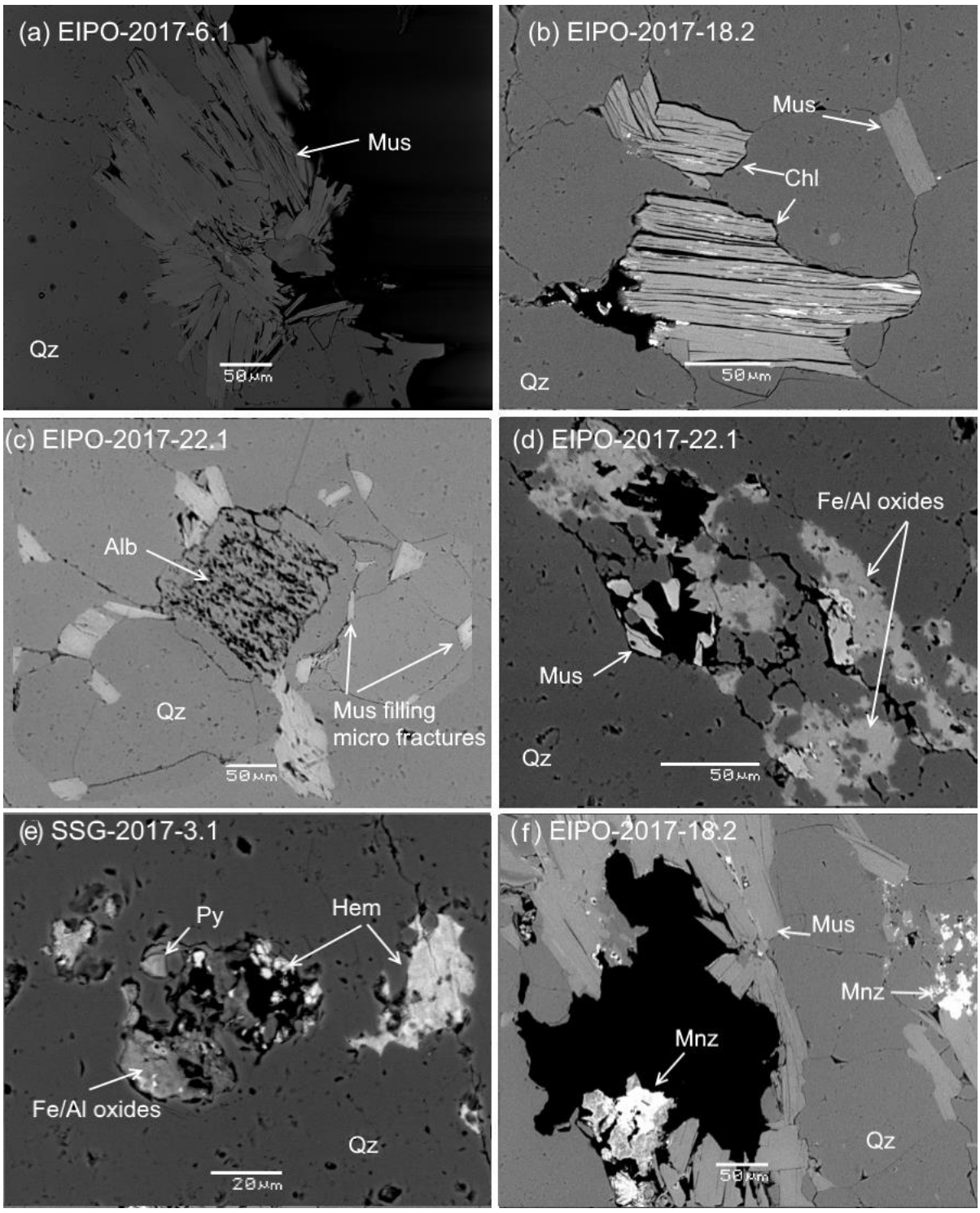

Figure 8. *SEM- images of quartz from the studied deposit; (a-c) Enrichment of muscovite (Mus) impurities at the grain boundary as well as in cracks and fracture-filling by muscovite and albite (Alb); (d, f) quartz replaced by hematite (Hem) and Al/Fe clay materials; (f) Cavities filling by muscovite (Mus) and monazite (Mnz).*

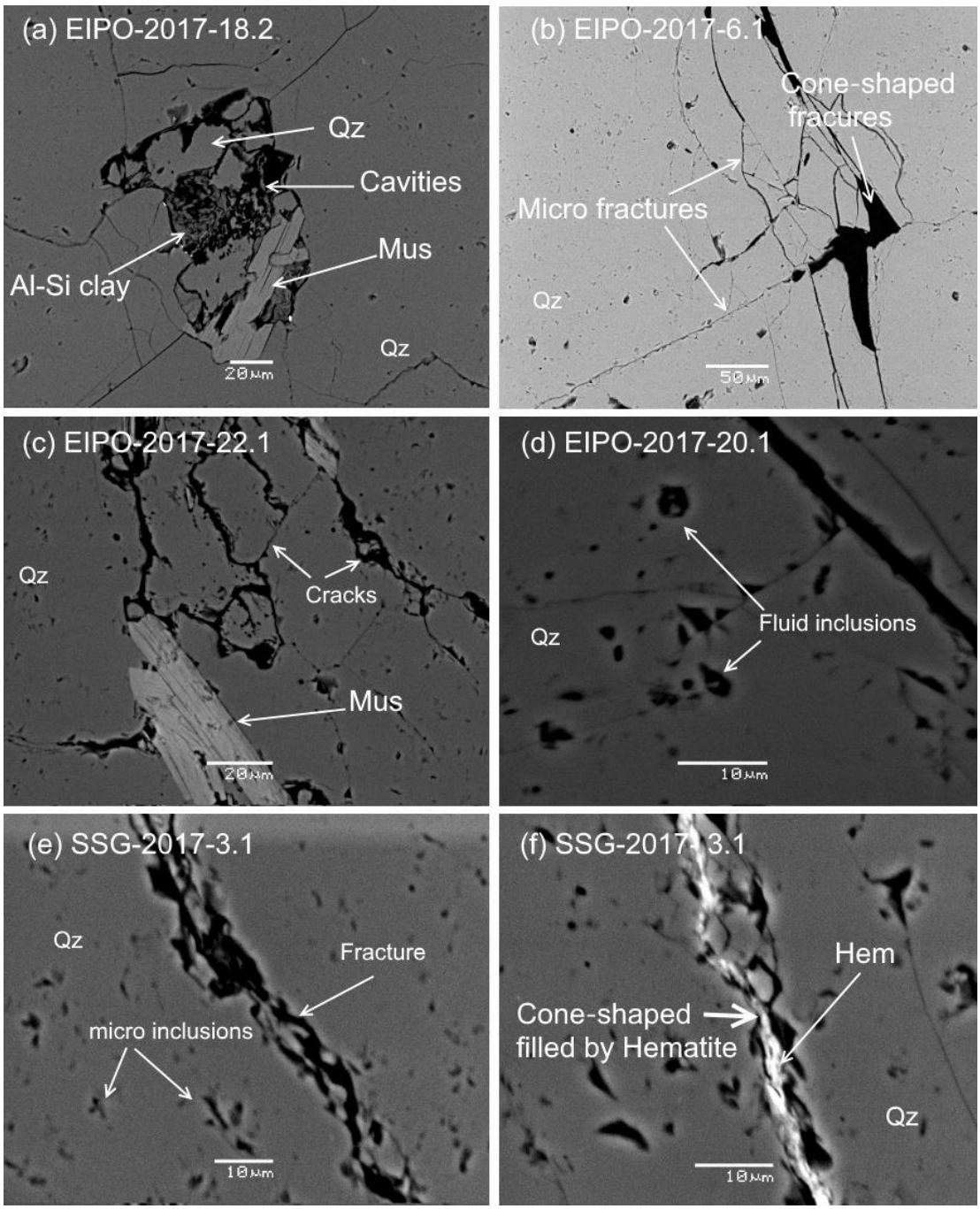

Figure 9. *SEM- images of quartz grain boundaries cavities (a) small depression meets with grain boundaries filled by clay; (b) Open grain boundary with cone-shaped cavities; (c) Cavities of variable shape generated by dissolution–precipitation processes; (d, e) Micrometer-sized depressions and fluid inclusions at sites where dislocation lines meet the open grain boundaries; (f) dissolution–precipitation processes with iron oxides (Hem) filling some fractures.*

Table 2. *EDS analyses of representative mineral composition of mineral impurities within quartz samples by SEM.*

Spectrum	Na_2O	MgO	Al_2O_3	SiO2	K_2O	CaO	MnO	Fe_2O_3	Total
Muscovite (Mus) 1	1.01	0.86	32.07	55.16	9.95			1.07	100
Muscovite (Mus) 2	0.68	1.39	30.94	55.57	9.59			2.11	100
Muscovite (Mus) 3	0.85	1.43	30.18	55.91	9.31			1.83	100
Albite (Alb) _1	10.5	1.06	18.63	69.81					100
Albite (Alb) _2	11.6	0.6	19.59	68.21					100
Albite (Alb) _3	9.96		15.74	74.16					
Hematite (Hem)_1		1.08	4.81	28.82			0.71	64.77	100
Hematite (Hem)_2			7.86	23.99			0.86	67.31	100
Hematite (Hem)_3			6.2	28.17			0.74	65.3	100
Al-Fe Clay_1		2.9	26.1	53.45	0.56	2.25		14.73	100
Al-Fe Clay_2		2.39	27.44	53.13	0.7	2.45		13.9	100
Al-Fe Clay_3		2.43	26.77	53.35	0.38	3.1		13.96	100

4.3 Whole-rock chemistry

Bulk rock chemical compositions of all investigated quartz samples determined by X-ray fluorescence spectrometry (XRF) and inductively coupled plasma mass spectrometry (ICP-MS) are summarized in Table 4. This analysis was aimed at finding out whether the total concentrations of these trace elements do not exceed 50 µg g-1 as required by the HPQ definition. The analyzed samples show Al, Fe, Mg and alkali metals Na and K concentrations were relatively high in some quartzite samples with fewer exceptions. Silica content, ranging from 92.6 to 95.85%, Fe (70-2660 ppm) and Al (106-8890 ppm). Al and Fe are predominantly clustered in foreign minerals present in the quartz and its oxidation state is influenced by its hosting mineral. In this specific case, Fe is present in distinct muscovite crystals and hematite with predominance of Fe^{3+}. Fe is affected by the decomposition of muscovite and it is found as Fe^{2+}; as muscovite disappears, Fe diffuses in the molten silica segregating towards interfaces. The most characteristic chemical features of the quartz samples are the low concentrations of K (25-3140 ppm), Na (222-1110 ppm), Ca (21-930 ppm), and Ti (20-110 ppm), i.e., totally less than 0.8 wt% (Fig. 10a). The concentrations of other trace elements Ba, Bi, Cr, Ga, Rb, S, Sb, Sr, Th, V, Zn and Zr are lower than the limit of detection.

Al and Ti are used as indicator elements of the quartz quality because they are the most common trace elements and they are difficult to remove during refinement of quartz. Al and Ti concentrations in studied quartz samples are plotted in logarithmic Al and Ti diagram according to Müller et al., 20007 for comparison with several Norwegian kyanite quartzite deposits and Swedish kyanite quartzite from Halsjöberget (Fig. 10b). Most of the analyses of quartz from selected potential High Purity Quartz (HPQ) deposits in Finland have significantly higher Al, Ti, K and Fe and plots in the low quality field. Low Al and Ti observed in some studied quartz samples such as M331390R350 33.55-33.65, EIPO-2017-7.1, EIPO-2017 20.1, SSG-2017-3.1 and SSG-2017-6.1, do not seem to be elevated Ti and Al concentrations, which plot at the boundary of the medium purity quartz field. However a beneficiation study on these deposits is recommended to establish possible industrial applications that may be feasible.

Table 3. *Modal mineralogy of mineral impurities determined by X-ray feature analysis, particle-by-particle and point count in scanning electron microscopy of quartz polished thin sections.*

Sample: EIPO-2017-6.1

Mineral	Grain Count	Mineral%
Quartz	3987	98.7
Muscovite	54	1.3
Total grain count	4041	100

Sample: EIPO-2017-7.1

Mineral	Grain Count	Mineral%
Quartz	4000	100
Fluid inclusions		
Total grain count	4000	100

Sample: EIPO-2017-20.1

Mineral	Grain Count	Mineral%
Quartz	4000	100
Fluid inclusions		
Total grain count	4000	100

Sample: EIPO-2017-22.1

Mineral	Grain Count	Mineral%
Quartz	3985	98.6 %
Muscovite	35	0.9 %
Albite	14	0.3 %
Al/Fe oxides (clay)	6	0.1 %
Total grain count	4040	100

Sample: EIPO-2017-18.2

Mineral	Grain Count	Mineral%
Quartz	3600	90.9
Muscovite	300	7.6
Albite	26	0.7
Al/Fe oxides (clay)	20	0.5
K-feldspar	10	0.3
Monazite	5	0.1
Total grain count	3961	100

Sample: SSG-2017-3.1

Mineral	Grain Count	Mineral%
Quartz	4063	99.3
Hematite	20	0.5
Al/Fe oxides (clay)	10	0.2
Total grain count	4093	100

Table 4. *Contents of main impurity elements within quartz samples collected from Central and Southern Finland.*

Sample	M243155R41 85.80-85.90	M331390R350 24.30-24.40	M331390R350 26.55-26.70	M331390R350 31.25-31.35	M331390R350 33.55-33.65	EIPO-2017 3.1	EIPO-2017 6.1	EIPO-2017 7.1
Al	423	265	265	265	265	2276	529	212
K	141	75	58	83	42	880	33	25
Ca	929	71	21	71	21	71	21	21
Ti	18	18	18	18	18	18	18	18
Fe	420	280	70	350	140	280	140	140
Na	297	223	223	223	223	297	223	223
Mg	181	121	121	121	121	121	121	121

Sample	EIPO-2017 9.1	EIPO-2017 9.2	EIPO-2017 13.1	EIPO-2017 18.1	EIPO-2017 18.2	EIPO-2017 20.1	EIPO-2017 22.1	EIPO-2017 24.1
Al	688	4128	2329	1270	8891	106	1164	2117
K	291	623	938	282	3138	42	465	1436
Ca	71	286	71	71	21	21	71	21
Ti	18	54	18	18	18	18	18	36
Fe	350	2658	699	210	1119	140	280	210
Na	223	223	223	668	1113	223	223	297
Mg	121	3739	784	121	543	121	121	121

Sample	EIPO-2017 28.1	EIPO-2017 28.2	SSG-2017 1.1	SSG-2017 2.1	SSG-2017 3.1	SSG-2017 4.1	SSG-2017 5.1	SSG-2017 6.1
Al	1217	2646	4869	476	106	8468	423	106
K	540	1752	2125	315	25	1320	183	25
Ca	21	21	929	21	21	21	21	21
Ti	18	42	108	18	18	42	18	18
Fe	210	490	699	140	140	769	280	70
Na	223	668	223	223	223	297	223	223
Mg	121	121	302	121	121	121	121	121

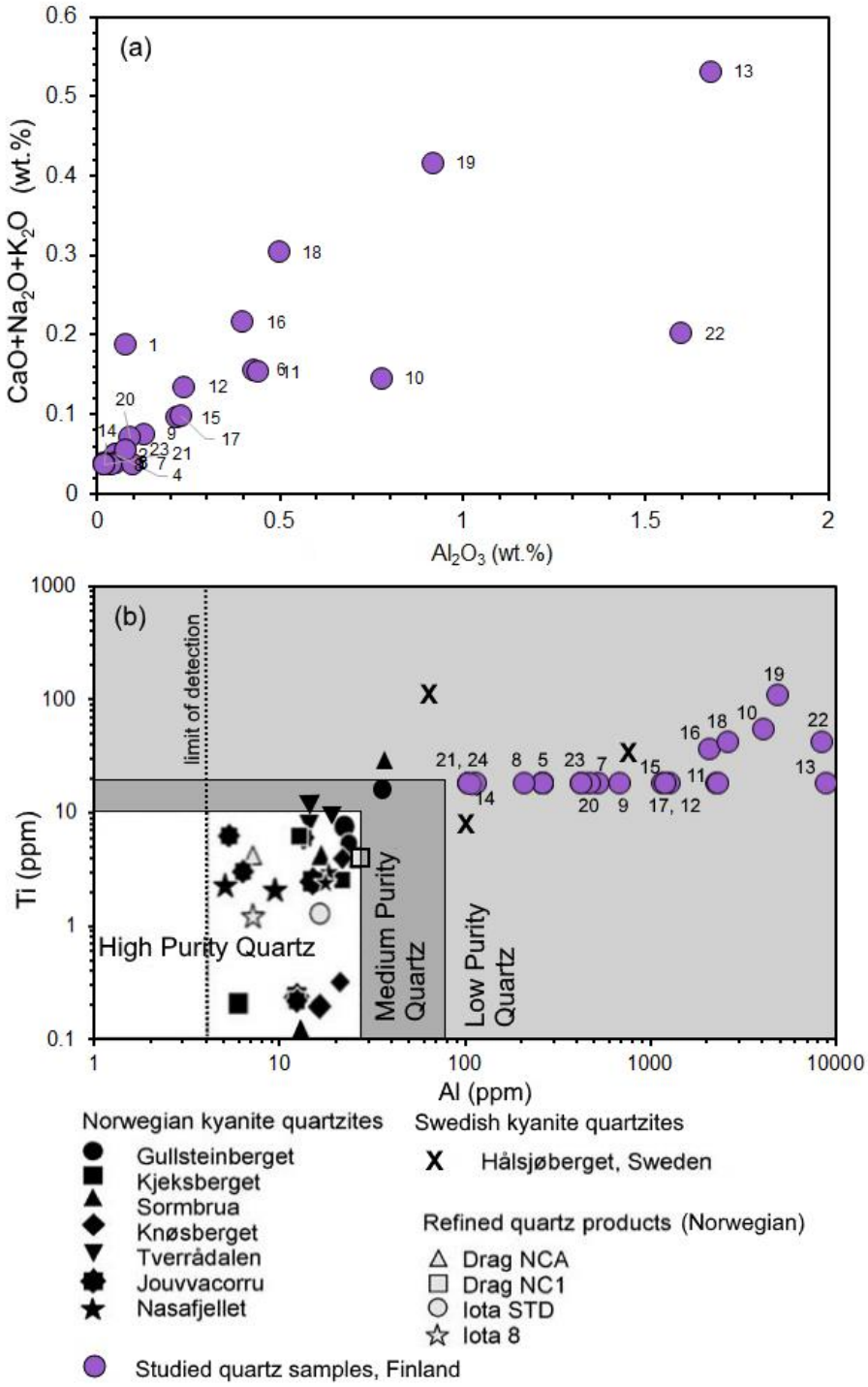

Figure 10. *(a) Major element plot of quartz samples collected from Central and Southern Finland; (b) Logarithmic Al vs Ti diagram of studied quartz in Finland compared to kyanite quartzite from Norway, Sweden and refined HPQ products from Norway (Müller et al., 2007). Quartz with Al <25 ppm and Ti <10 ppm is considered as high-purity quartz HPQ.*

4.4 High-resolution X-ray computed microtomography

X-ray micro-CT offers the advantages of non-destructive imaging of relatively large areas of high spatial resolution and can be used to feed micromechanical models. After reconstructing the 3D distribution of X-ray attenuations, the contrasting grayscale spectrum allowed us to segment and separate high-purity quartz and their inclusions, mainly muscovite, albite and clay. The 3D images were processed using the PerGeos software (https://www.thermofisher.com/fi/en/home/industrial/electron-microscopy/electron-microscopy-instruments-workflow-solutions/3d-visualization-analysis-software/pergeos-digital-rock-analysis.html). The grayscale values of the voxels in the reconstructed image are dependent on the density or concentration of matter in the corresponding volume. Microtomography scan of a micro piece, cut from the quartz sample (3 × 1.5 × 15 mm diameter), exhibits contrasting grayscale spectrum, which allowed us to segment and separate high- purity quartz and their inclusions, mainly muscovite, albite and clay (Fig. 10a-d). X-ray m-CT image of quartz sample is presented in Figures 10a-d where a, b) show cross-sections of the samples in grey scale. Based on the density contrast, muscovite impurities were separated from the pure quartz, which mostly appear as bright in the grey spectrum and needle-like shape (Fig.10d).

Furthermore, the high-purity quartz contains different generations of fluid and melt inclusions which, trapped within the crystallographic orientation of quartz, healed cracks and micro fissures. For our investigations here we have chosen four different quartz crystal samples of a size of 3 mm and vertical orientation (Fig.11a). Figure (11b) reveals fluid and melt inclusions appear either as ***pore*-lining** aggregates along healed micro-fractures terminating at the edge of a single quartz grain or as ***irregular clusters*** in quartz grains. These inclusions or pores may contain gas and liquid and sometimes even very small crystals. Thus, the high-resolution XCT imaging reveals the internal structure of the studied quartz samples which are viewed as High Purity Quartz (HPQ). XCT allows us to identify > 4 μm fluid inclusions while the identification and volumetric reconstruction of the different phases can be carried out with reasonable confidence for relatively large (> 25 μm) inclusions. Density contrasts are high enough to properly identify the aqueous mono phase (liquid) and two-phase (liquid+vapor) fluid inclusions with 5 to 25 μm sizes. The 3D spatial distribution of crystallised fluid inclusion and pores are represented in blue, as shown in Figure (11b). The volumetric reconstruction of the liquid and vapor phases or porosity values calculated from the XRCT images of four quartz samples are 0.87 %, 0.34 %, 0.16 % and 0.13 % respectively, with a mean value less than 1 %.

North-south and east-west vertical sections (Fig. 11d) cutting quartz crystal reveals the presence of different mineral impurities and voids in the quartz matrix. Figure 11d shows the images are taken from each section as high-resolution scans, and distribution of muscovite impurities and fluid inclusions present in the quartz sample identified with a different colour.

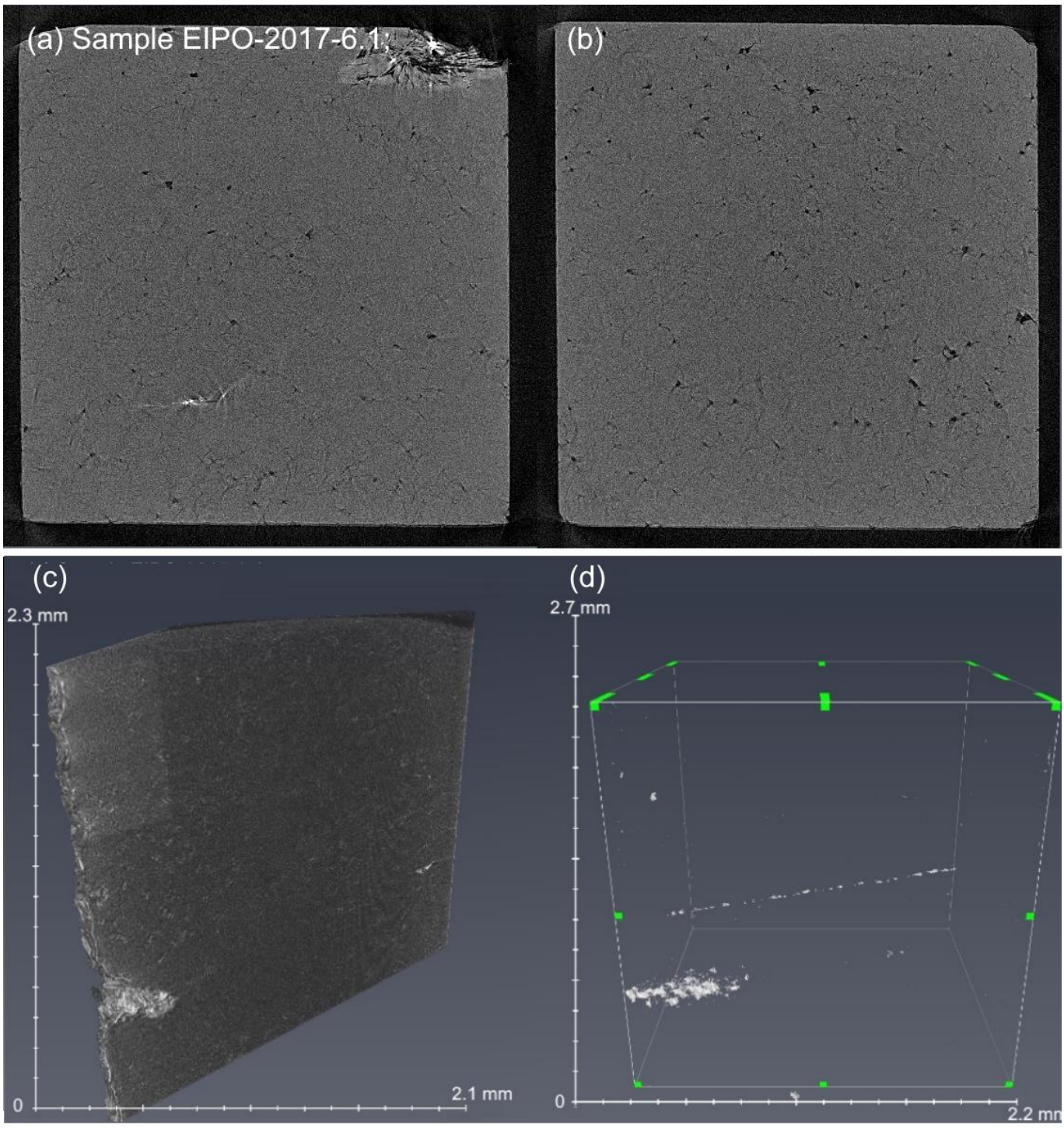

Figure 10. *X-ray computed tomography images of quartz sample EIPO-2017-6.1; (a, b) X-ray μ-CT images show a cross-section of the sample in gray scale; (c) 3D-XCT image of the quartz sample; (b, d) Rendered XCT image showing the preferred orientation of muscovite impurities in bright colour.*

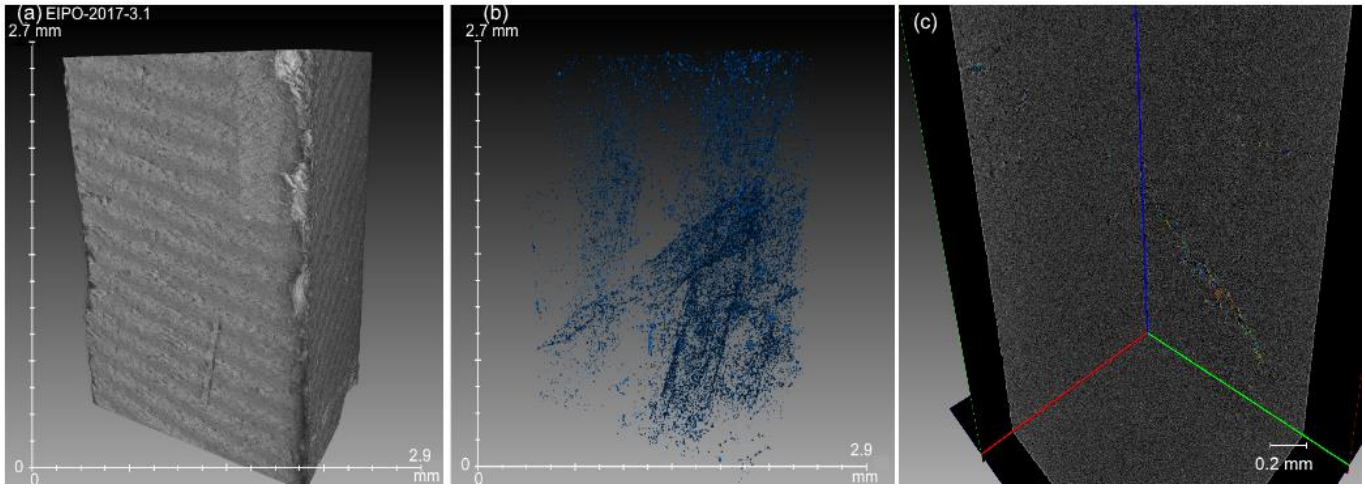

Figure 11. *X-ray computed tomography images of quartz sample EIPO-2017-3.1; (a) 3D- XCT images show the surface of the sample in grayscale; (b) 3D-XCT image of the quartz sample showing the pore-lining aggregates along healed micro-fractures and as irregular clusters in quartz sample; (c) 2D cross-sections, showing the distribution of mineral impurities in different colour.*

5 CONCLUSION

The quartz samples of different genetic types (hydrothermal, pegmatite, and quartzite) from 18 localities in the Central and Southern Finland have been characterized in detail by microscopic optical techniques, SEM, trace-element analysis by XRF and ICP-MS, as well as X-ray tomography. Various mineral impurities inclusions such as muscovite, albite, K-feldspar, Al/Fe oxides (clay), and secondary fluid inclusions have been detected. Elevated concentrations of selected trace elements such as Al (106-8890 ppm), K (25-3140 ppm), Fe (70-2660 ppm), Mg (120-3740), Na (222-1110 ppm), Ca (21-930 ppm), and Ti (20-110 ppm) that were analysed by XRF could be related to minerals (Muscovite, albite, etc.) and fluid (Na, K, Ca, Mg) micro-inclusions.

The volume percentage of liquid and vapor phases or porosity, as well as impurity inclusions, are determined by X-ray tomographic study and are found to be 0.87 %, 0.34 %, 0.16 % and 0.13 % respectively.

This report reviews general aspects of high purity quartz deposits, exploration requirements, quality evaluation of raw quartz, and provides detailed investigations of the specific impurities ubiquitously found in quartz samples. Most of quartz samples under this study do not meet the requirements of the HPQ definition and are thus not HPQ deposits. However a beneficiation study on these deposits is recommended to establish possible industrial applications that may be feasible.

6 REFERNCES

Cnudde, V., and Boone, M.N., 2013, High resolution X-ray computed tomography in geosciences: A review of the current technology and applications: Earth-Science Reviews, v. 123, p. 1–17, doi: 10.1016 /j .earscirev.2013.04.003.

Dal Martello E, et al., 2011a. Electrical fragmentation as a novel refining route for hydrothermal quartz for SoG-Si production. Miner Eng. doi: 10.1016/j.powtec.2012.02.055.

Dal Martello E, et al., 2011b. Study of pellets and lumps as raw materials in silicon production from quartz and silicon carbide. Metall Mater Trans B, p. 12.

Götze, J., 2009. Chemistry, textures and physical properties of quartz geological interpretation and technical application. Mineral Mag 73, 645–671.

Haus, R., 2010. High-purity quartz resources. In: PHOTON0s 8th solar silicon conference.

IOTA®, 2005. IOTA® high-purity quartz. Accessed 20th May 2005, http://www.iotaquartz.com/welcome.html

Ketcham, R.A., and Carlson, W.D., 2001, Acquisition, optimization and interpretation of X-ray computed tomographic imagery: Applications to the geosciences: Computers & Geosciences, v. 27, p. 381–400, doi: 10.1016/S0098-3004 (00) 00116-3.

Kilias, S., Voudouris, P., Katerinopoulos, A., Kavouri S., 2004. “Study of fluid inclusions in alpine type quartz from discontinuity joints of Pentelic Mountain.” Proceedings of the 10th International Congress, Thessaloniki, April 2004.

Mancktelow, N.S., Pennacchioni, G., 2004. The influence of grain boundary fluids on the microstructure of quartz-feldspar mylonites, Journal of Structural Geology, 26(1):47-69, DOI: 10.1016/S0191-8141(03)00081-6

Moore, P., 2005. High-purity quartz. Ind Miner 455:53–57.

Müller, A., Ihlen, P.M., Wanvik, J.E. 2007. High-purity quartz mineralisation in kyanite quartzites, Norway, Miner Deposita, 42:523–535, DOI 10.1007/s00126-007-0124-8

Nestola, F., Merli, M., Nimis, P., Parisatto, M., Kopylova, M., De Stefano, A., Longo, M., Ziberna, L., and Manghnani, M., 2012. In situ analysis of garnet inclusion in diamond using single-crystal X-ray diffraction and X-ray micro-tomography. European Journal of Mineralogy, 24(4), 599–606.

Norwegian Crystallites AS., 2006. Norwegian Crystallites AS-products-crystal quartz analyses. Accessed 20th September 2006. http://www.norcryst.no.

Parisatto, M. et al., 2018. Three-dimensional distribution of primary melt inclusions in garnets by X-ray microtomography, American Mineralogist 103, 911–926.

Roedder, E., 1984. Fluid inclusions. Reviews in Mineralogy. Mineral. Soc. America, Washington., v.12, 644p.

Sayab, et al., 2015. High resolution X-ray computed micro tomography: A holistic approach to metamorphic fabric analyses: Geology, v. 43, p. 55–58, doi: 10 .1130 /G36250.

Sayab, M., et al., 2016. Three-dimensional textural and quantitative analyses of orogenic gold at the nanoscale, Geology, v. 44, p. 739–742, doi:10.1130/G38074.1.

Sayab, M., et al., 2017. Orthogonal switching of AMS axes during type-2 fold interference: Insights from integrated X-ray computed tomography, AMS and 3D petrography. Journal of Structural Geology, 103, 1-16. doi:10.1016/j.jsg.2017.09.002.